AIP | Applied Physics Letters

Diamagnetic particle separation by shape in ferrofluids

Yilong Zhou and Xiangchun Xuan

Citation: Applied Physics Letters **109**, 102405 (2016); doi: 10.1063/1.4962638
View online: http://dx.doi.org/10.1063/1.4962638
View Table of Contents: http://scitation.aip.org/content/aip/journal/apl/109/10?ver=pdfcov
Published by the AIP Publishing

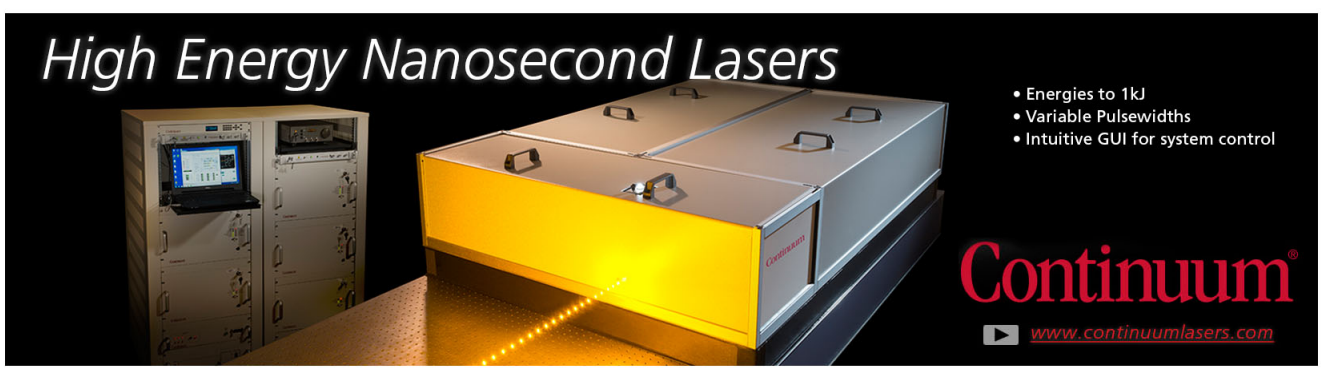

Diamagnetic particle separation by shape in ferrofluids

Yilong Zhou and Xiangchun Xuan[a)]
Department of Mechanical Engineering, Clemson University, Clemson, South Carolina 29634-0921, USA

(Received 15 July 2016; accepted 30 August 2016; published online 9 September 2016)

Separating particles, which can be either biological or synthetic, in a continuous label-free manner is essential to many applications. Magnetic separation has several advantages over other field-driven particle separation techniques. It, however, has been limited primarily to situations where particles differ in size or magnetization. We demonstrate in this paper a continuous-flow separation of equal-volumed spherical and peanut-shaped diamagnetic particles in a dilute ferrofluid. This separation is attributed to the shape-dependent magnetophoretic motion, which is the combined result of the shape dependences of the magnetic force and viscous drag. We also develop a three-dimensional numerical model to understand this shape-based diamagnetic particle separation and predict the effects of the determining factors. *Published by AIP Publishing.*
[http://dx.doi.org/10.1063/1.4962638]

Separating particles and cells in a continuous label-free manner is essential to many chemical, biomedical, and environmental applications.[1–5] Magnetic separation[6–10] has several advantages over other field-driven techniques (e.g., electric,[11,12] acoustic,[13,14] optical,[15,16] and hydrodynamic[17,18] fields) such as simplicity and low-cost.[19–21] It utilizes the magnetic field gradient-induced magnetophoresis, which can be either towards (i.e., *positive* magnetophoresis for magnetic particles or magnetically tagged cells[22–27]) or away from (i.e., *negative* magnetophoresis for diamagnetic particles and cells in magnetic fluids[28–38]) the magnetic source, to separate particles and cells based on the difference in intrinsic properties. The existing studies in this area have so far been focused primarily upon the magnetic separation of particles and cells by size or magnetization.[6–10] We demonstrate in this work that magnetophoresis is also a function of particle shape, which can be exploited for a label-free magnetic separation.

Shape, which is an important property of particles and cells,[39,40] provides useful information for cell synchronization,[41] disease diagnostics,[42] etc. Shape-based particle and cell separation has been implemented via hydrodynamic filtration[43] in a complex network of microchannels[44] or deterministic lateral displacement in a high-resolution array of posts.[45,46] It has also been demonstrated through electrode-[41] or insulator-based[47] dielectrophoresis, which suffers from the issues of low throughput, potential cell damages, etc. Inertial[48] and elasto-inertial[49,50] focusing are both high-throughput methods that have been recently developed to separate particles and cells by shape through the use of the flow-induced lift force. In addition, the ac field frequency-dependent magnetic force and torque have been utilized to trap and circulate sickle and healthy red blood cells, respectively, in a custom-fabricated biocompatible ferrofluid for a shape-based separation.[51] We present in this work a continuous-flow separation of equal-volumed spherical and peanut-shaped diamagnetic particles in a diluted commercially available ferrofluid. We also develop a 3D numerical model to understand and predict this shape-based magnetic field-driven particle separation.

Fig. 1(a) shows a picture of the microfluidic chip, which was fabricated with polydimethylsiloxane (PDMS) using a custom-modified soft lithography method detailed elsewhere.[52] The T-shaped microchannel is uniformly 100 μm wide and 25 μm deep. It is composed of two 8 mm long side-branches (for the supply of particle mixture and ferrofluid sheath, respectively) and one 12 mm long main-branch (for particle separation). A neodymium-iron-boron permanent magnet (B421, $1/4'' \times 1/8'' \times 1/16''$, K&J Magnets, Inc.) is embedded into the PDMS slab, and positioned 1 mm away from the main-branch, 2.5 mm away from the side-branch. Its magnetization direction is through the $1/16''$ thickness and perpendicular to the main-branch. Fig. 1(b) shows a zoom-in image of 6 μm-diameter fluorescent spherical (Phosphorex,

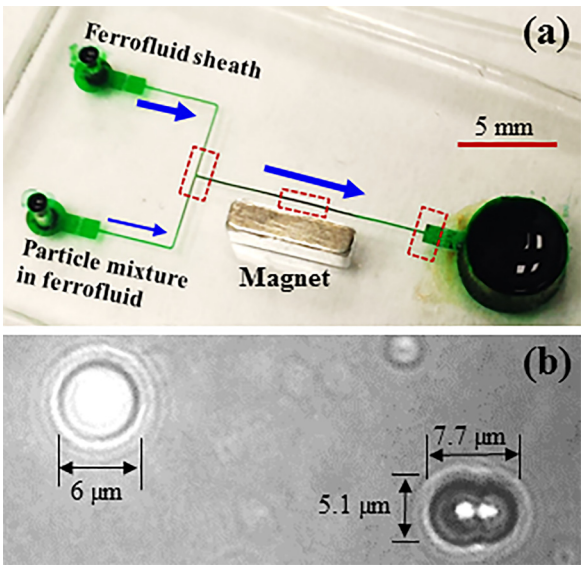

FIG. 1. (a) Picture of the PDMS-based microfluidic chip used in experiments. The three dashed-line boxes highlight the windows of view for observing particle motions. The block arrows indicate the flow directions during particle separation. (b) Zoom-in image of one fluorescent spherical (left, white) and one plain peanut-shaped (right, black) diamagnetic polystyrene particle with the dimensions being labeled.

[a)]Author to whom correspondence should be addressed. Electronic mail: xcxuan@clemson.edu. Fax: 864-656-7299.

Inc.) and 5.1 μm-diameter/7.7 μm-length plain peanut-shaped (Magsphere, Inc.) diamagnetic polystyrene particles for shape-based separation. The peanut particle is a result of the fusion of two 5.1 μm-diameter spherical particles, whose overall volume was calculated to be 117.62 μm^3 using the geometry package in COMSOL®. This volume corresponds to an equivalent spherical diameter of 6.08 μm, which deviates from that of the spherical particle by 1.33%. These two types of particles were mixed and re-suspended in 0.3× EMG 408 ferrofluid (Ferrotec Corp., diluted by water). A pure 0.3× EMG 408 ferrofluid was used as the sheath fluid to pre-focus the particle mixture at the T-junction of the microchannel. Other experimental details are referred to in our recent paper.[52]

The mixture of spherical and peanut-shaped particles is pre-focused to a tight stream along the sidewall of the main-branch that is nearer to the magnet. These diamagnetic particles each experiences a magnetic force, $\mathbf{F}_m$, in the ferrofluid and is pushed away from the magnet[53]

$$\mathbf{F}_m = -\mu_0 V_p (\mathbf{M}_f \cdot \nabla)\mathbf{H}/(S_m O_m), \tag{1}$$

where μ_0 is the permeability of the free space, V_p is the volume of the particle, $\mathbf{M}_f$ is the magnetization of the ferrofluid, $\mathbf{H}$ is the magnetic field at the particle center, S_m is the particle shape-dependent demagnetizing factor that is 1 for a spherical particle and increases with the particle non-sphericity,[54] and O_m is the particle orientation-dependent correction factor that reduces to 1 for a spherical particle or when the major axis of a non-spherical particle aligns with the magnetic field line.[55] Note that the contribution of the magnetization of diamagnetic particles has been neglected in Eq. (1) because the magnetic susceptibility of polystyrene particles (on the order of 10^{-6})[56–58] is at least 4 orders of magnitude smaller than that of the ferrofluid we used in the experiment (on the order of 0.1, Ferrotec Corp.[59]). To further verify this assumption, we have compared the magnetic susceptibilities of the two types of particles in water using the microfluidic chip in Fig. 1(a). No visible deflection was observed for either type of particles under the action of a permanent magnet. This experiment indicates that the magnetic susceptibilities of the spherical and peanut-shaped polystyrene particles are both negligible and should have no contributions to the demonstrated separation in the ferrofluid.

The magnetic force, $\mathbf{F}_m$, acting on a particle is balanced instantly by the viscous drag force in low Reynolds number flows (to be explained later), $\mathbf{F}_d$[60]

$$\mathbf{F}_d = 3\pi\eta d_p(\mathbf{u}_f - \mathbf{u}_p) f_D S_d O_d, \tag{2}$$

where η is the ferrofluid viscosity, d_p is the (equivalent) spherical diameter of the particle, $\mathbf{u}_f$ is the ferrofluid velocity, $\mathbf{u}_p$ is the particle velocity, f_D is the drag coefficient accounting for the wall retardation effects,[60] S_d is the particle shape-dependent correction factor that is equal to 1 for a spherical particle and increases with the particle non-sphericity, and O_d is the particle orientation-dependent correction factor which decreases to 1 for a spherical particle or when the motion of a non-spherical particle is along the direction of its major axis.[60–62] The resulting particle velocity is given by

$$\mathbf{u}_p = \mathbf{u}_f - \frac{\mu_0 d_p^2 (\mathbf{M}_f \cdot \nabla)\mathbf{H}}{18\eta f_D G_i}, \tag{3}$$

where $G_i = S_m O_m S_d O_d \geq 1$ is the lumped correction factor for the combined effects of particle shape (i.e., S_m and S_d) and orientation (i.e., O_m and O_d) on magnetophoresis that becomes 1 for spherical particles. It is the dependence of $\mathbf{u}_p$, more accurately, the cross-stream negative magnetophoretic motion in the second term on the right hand side of Eq. (3), on particle shape that enables the continuous diamagnetic particle separation. Specifically, spherical particles can be deflected away from the magnet at a higher rate than non-spherical particles of equal volume due to the former's smaller value of G_i.

A 3D numerical model was developed to simulate the transport and separation of spherical and peanut-shaped diamagnetic particles in the ferrofluid. It was solved in COMSOL 5.1, and the details are referred to in our recent paper.[35] Briefly, the Laminar Flow module was employed to solve for the flow field, $\mathbf{u}_f$, and the intrinsic Streamline function was used to trace particles via the particle velocity, $\mathbf{u}_p$, in Eq. (3). The magnetic field was obtained directly from Furlani's analytical formulae for rectangular magnets[63] (see the magnetic field contour in Fig. S1 of the supplementary material). The value of the lumped correction factor, G_i, in Eq. (3) for the magnetophoretic motion of peanut particles was determined by matching the predicted trajectories with the experimentally obtained streak images.

Fig. 2 demonstrates the separation of equal-volumed spherical (fluorescent) and peanut-shaped (plain) diamagnetic particles in 0.3× EMG 408 ferrofluid through the T-shaped microchannel (see movies in the supplementary material). The volumetric flow rates are 6 μl/h and 120 μl/h for the

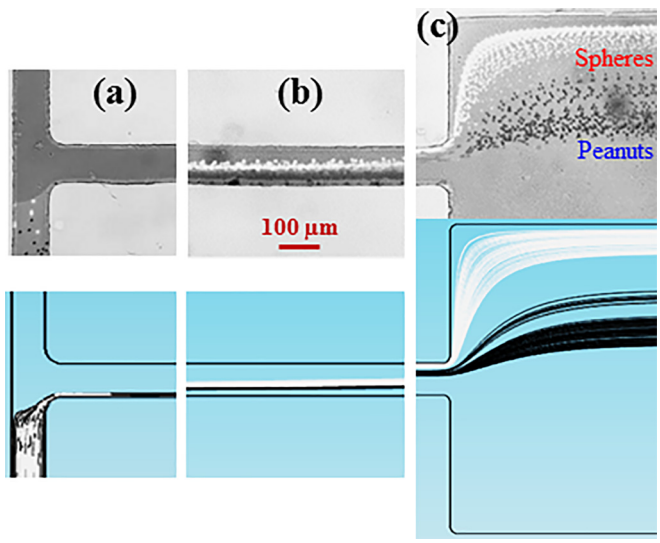

FIG. 2. Illustration of the shape-based separation of spherical (fluorescent) and peanut-shaped (plain) diamagnetic particles in 0.3× EMG 408 ferrofluid through the T-shaped microchannel. The top row shows the snapshot image at the T-junction (a), composite image at the middle of the main-branch (b), and composite image at the expansion of the main-branch (c). The bottom row shows the numerically predicted particle trajectories (white lines for fluorescent spheres and black lines for plain peanuts). Note that part of the experiment image in (c) is covered by the numerical image. The flow rates of the particle mixture solution and ferrofluid sheath are 6 μl/h and 120 μl/h, respectively.

particle mixture solution and sheath ferrofluid, respectively. As viewed from the snapshot image at the T-junction in Fig. 2(a), the two types of particles are uniformly mixed in the side-branch and focused to a tight stream along the sidewall of the main-branch that is closer to the magnet [see also Fig. 1(a)]. They are then both pushed away from the sidewall by negative magnetophoresis at a shape-dependent rate. The composite particle image at the middle of the main-branch in Fig. 2(b), which was obtained by stacking the two superimposed images for fluorescent and plain particles through background subtraction, indicates that the spherical (fluorescent) particles migrate at a larger rate than the peanut (plain) particles. The result of this shape-dependent cross-stream magnetophoretic motion is a continuous separation of the two particle sub-streams, which is further enhanced at the expansion of the main-branch due to the local hydrodynamic spreading[50] as illustrated by the composite image in Fig. 2(c). The numerically predicted trajectories of the spherical (white lines) and peanut-shaped (black lines) particles under the experimental conditions are shown in the bottom row of Fig. 2. The lumped correction factor, G_i, in Eq. (3) was set to 1.4 for the peanut particles in the model. Note that this same value was also used in all other case studies to be presented later. The simulation and experimental results agree with each other in all three windows of view.

To further verify that the demonstrated particle separation in Fig. 2 is indeed a result of the shape-dependent magnetophoretic motion, we did a control experiment where the magnet was removed while all other experimental conditions were maintained (see movies in the supplementary material). The spherical and peanut-shaped particles were observed to move out of the main-branch in a still uniformly mixed stream without any separation (see also the experimental images in Fig. S2 of the supplementary material). Moreover, there is no visible displacement from the sidewall of the main-branch for either type of particles after the pre-focusing, which indicates a negligible influence of inertial lift[64,65] at low Reynolds number ($Re = \rho V D_h/\eta \approx 0.6$ where $\rho = 1.05 \times 10^3$ kg/m^3 is the ferrofluid density, $V = 14$ mm/s is the average fluid velocity in the main-branch, $D_h = 40$ μm is the channel's hydraulic diameter, and $\eta = 1.03 \times 10^{-3}$ kg/m s is the ferrofluid viscosity) flows. This control experiment also indicates an insignificant contribution from the particle steric effects in pinched flow fractionation.[66] It is because the stream width of the pre-focused particle solution, which is around 10 μm from our 3D flow simulation at the flow rate ratio, $\alpha = Q_s/Q_p = 20$ (Q_s and Q_p are the volumetric flow rates of the ferrofluid sheath and particle mixture, respectively), is greater than any dimension of the two types of particles. The above analysis is validated by the close agreement between the experimental observations and numerical predictions in all three windows of view (see Fig. S2 in the supplementary material).

Fig. 3 shows the effect of flow rate on the shape-based separation of diamagnetic spherical and peanut particles in 0.3× EMG 408 ferrofluid at the expansion of the main-branch. The volume flow rate of the sheath ferrofluid is varied from $Q_s = 80$ μl/h to 160 μl/h at a fixed sheath-fluid to particle-mixture flow rate ratio, $\alpha = 20$. As seen from the superimposed images and PDF plot in Fig. 3(a), both types of particles achieve a (nearly) full channel-width deflection at $Q_s = 80$ μl/h and hence still mix with each other at the expansion of the main-branch. This happens because the particles in a low-velocity flow have a sufficiently long residence time to undergo the magnetophoretic migration across the flow in the main-branch. At an increased flow rate of $Q_s = 120$ μl/h, spherical particles can still (almost) reach the sidewall while the peanut particles are about one quarter of the channel width behind. Thus, a clear gap is formed in between the two particle sub-streams as viewed from both the superimposed images and the PDF plot in Fig. 3(b). Further increasing the flow rate, however, makes the residence time in the main-branch short for both types of particles, which reduces not only the absolute but also the relative displacement of the two types of particles. Moreover, the span of each particle sub-stream increases with the increasing flow rate due to the fluid velocity gradients induced particle dispersion in the channel depth direction (note the sheath fluid focuses particles in the channel width direction only). Therefore, the particle separation gets worse at $Q_s = 160$ μl/h as shown in Fig. 3(c). The experimentally observed diamagnetic particle deflection, dispersion, and separation are predicted by the 3D numerical model with a good agreement for all three values of Q_s in Fig. 3.

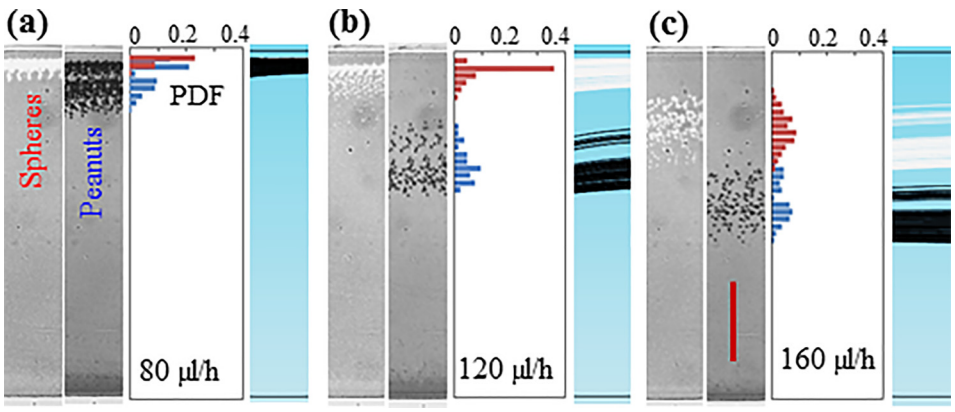

FIG. 3. Flow rate effects on the shape-based separation of spherical (fluorescent) and peanut-shaped (plain) diamagnetic particles in 0.3× EMG 408 ferrofluid. The volume flow rate of the sheath ferrofluid is varied from 80 μl/h (a) to 120 μl/h (b) and 160 μl/h (c) while the flow rate ratio between the sheath fluid and particle mixture is fixed at $\alpha = 20$. Each panel shows from left to right the superimposed image of spherical particles, superimposed image of peanut-shaped particles, plot of particle PDF, and numerically predicted particle trajectories (white lines for fluorescent spheres and black lines for plain peanuts) at the expansion of the main-branch. The scale bar represents 200 μm.

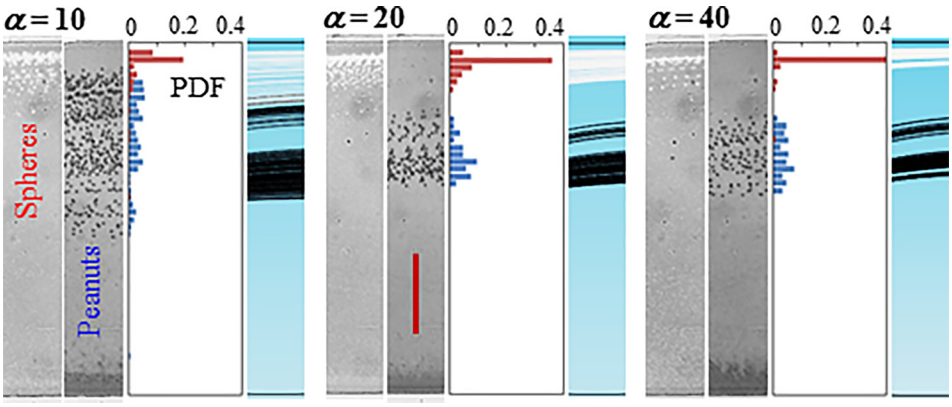

FIG. 4. Flow rate ratio effects on the shape-based separation of spherical (fluorescent) and peanut-shaped (plain) diamagnetic particles in 0.3× EMG 408 ferrofluid. The volume flow rate of the sheath ferrofluid is fixed at 120 μl/h while that of the particle mixing is varied from 12 μl/h (i.e., with a flow rate ratio of $\alpha = 10$) to 6 μl/h (i.e., $\alpha = 20$) and 3 μl/h (i.e., $\alpha = 40$). Other details on the set-up of each panel are referred to the caption of Fig. 3.

Fig. 4 shows the effect of sheath ferrofluid to particle mixture flow rate ratio, α, on the shape-based separation of diamagnetic spherical and peanut particles. The volume flow rate of the sheath fluid is fixed at 120 μl/h while that of the particle mixture is varied from 12 μl/h (i.e., $\alpha = 10$) to 3 μl/h (i.e., $\alpha = 40$). As α increases, the total flow rate in the main-branch of the microchannel slightly decreases (by less than 10%), yielding an almost unvaried residence time for the particles. Therefore, the magnetophoretic deflection of either type of particles remains approximately constant as viewed from the superimposed particle images in Fig. 4. However, the span of each particle sub-stream becomes smaller due to the enhanced focusing effect at the T-junction (data not shown) with the increasing α. This reduced particle dispersion acts to enhance the shape-based diamagnetic particle separation, which is demonstrated by the particle PDF plots in Fig. 4. The experimentally observed particle behaviors at the expansion of the main-branch are reasonably predicted by the 3D numerical model except for the under-predicted particle dispersion at $\alpha = 10$. This is probably due to the higher flow rate of particle mixture and hence a greater particle concentration in the main-branch at this smaller flow rate ratio. More frequent particle-particle interactions are thus present in the experiment and expected to cause an increase in particle dispersion, which is not considered in our numerical model.

In summary, we have demonstrated a continuous shape-based separation of equal-volumed spherical and peanut particles in a dilute ferrofluid. The particle mixture is pre-focused to a tight stream by a sheath ferrofluid, which is then split into two sub-streams due to the shape-dependent cross-stream magnetophoretic motion. The effects of flow rate and flow rate ratio between the sheath fluid and particle mixture are experimentally studied on this separation. We have also developed a 3D numerical model to simulate the particle trajectories in the ferrofluid through the T-shaped microchannel under the experimental conditions. With an experimentally determined correction factor for peanut-shaped particles, this model is able to predict the experimentally observed particle deflection, dispersion, and separation in all case studies with a reasonable agreement.

See supplementary material for details on the 3D contour of magnetic field in the computational domain, the experimental/numerical results of the control experiment for the shape-based diamagnetic particle separation in the absence of the magnet, and the movies for the shape-based separation with and without the magnet in three windows of view.

This work was supported in part by NSF under Grant No. CBET-1150670.

[1]N. Pamme, Lab Chip **7**, 1644–1659 (2007).
[2]D. R. Gossett, W. M. Weaver, A. J. Mach, S. C. Hur, H. T. Tse, W. Lee, H. Amini, and D. Di Carlo, Anal. Bioanal. Chem. **397**, 3249–3267 (2010).
[3]A. Karimi, S. Yazai, and A. M. Ardekani, Biomicrofluidics **7**, 021501 (2013).
[4]P. Sajeesh and A. K. Sen, Microfluid. Nanofluid. **17**, 1–52 (2014).
[5]C. W. Shields IV, C. D. Reyes, and G. P. Lopez, Lab Chip **15**, 1230–1249 (2015).
[6]N. Pamme, Lab Chip **6**, 24–38 (2006).
[7]M. Suwa and H. Watarai, Anal. Chim. Acta **690**, 137–147 (2011).
[8]Q. Cao, X. Han, and L. Li, Lab Chip **14**, 2762–2777 (2014).
[9]M. Hejazian, W. H. Li, and N. T. Nguyen, Lab Chip **15**, 959–970 (2015).
[10]W. Zhao, R. Cheng, J. Miller, and L. Mao, Adv. Funct. Mater. **26**, 3916–3932 (2016).
[11]R. Pethig, Biomicrofluidics **4**, 022811 (2010).
[12]J. Regtmeier, R. Eichhorn, M. Viefhues, L. Ogunovic, and D. Anselmetti, Electrophoresis **32**, 2253–2273 (2011).
[13]T. Laurell, F. Peterson, and A. Nilsson, Chem. Soc. Rev. **36**, 492–506 (2007).
[14]S. Lin, X. Mao, and T. Huang, Lab Chip **12**, 2766–2770 (2012).
[15]S. H. Cho, J. M. Godin, C. Chen, W. Qiao, H. Lee, and Y. Lo, Biomicrofluidics **4**, 043001 (2010).
[16]A. A. Kayani, K. Khoshmanesh, S. A. Ward, A. Mitchell, and K. Kalantar-zadeh, Biomicrofluidics **6**, 031501 (2012).
[17]H. Tsutsui and C. M. Ho, Mech. Res. Commun. **36**, 92–103 (2009).
[18]H. Amini, W. Lee, and D. Di Carlo, Lab Chip **14**, 2739–2761 (2014).
[19]M. A. M. Gijs, F. Lacharme, and U. Lehmann, Chem. Rev. **110**, 1518–1563 (2010).
[20]N. T. Nguyen, Microfluid. Nanofluid. **12**, 1–16 (2012).
[21]R. J. Yang, H. H. Hou, Y. N. Wang, and L. M. Fu, Sens. Actuators, B **224**, 1–15 (2016).
[22]D. W. Inglis, R. Riehn, R. H. Austin, and J. C. Sturm, Appl. Phys. Lett. **85**, 5093–5095 (2004).
[23]E. Mirowski, J. Moreland, A. Zhang, S. E. Russek, and M. J. Donahue, Appl. Phys. Lett. **86**, 243901 (2005).
[24]D. W. Inglis, R. Riehn, J. C. Sturm, and R. H. Austin, J. Appl. Phys. **99**, 08K101 (2006).
[25]J. D. Adams, P. Thévoz, H. Shea, H. Bruus, and H. T. Soh, Appl. Phys. Lett. **95**, 254103 (2009).
[26]K. Hoshino, Y. Y. Huang, N. Lane, M. Huebschman, J. W. Uhr, E. P. Frenkel, and X. Zhang, Lab Chip **11**, 3449–3457 (2011).
[27]J. H. Kang, S. Krause, H. Tobin, A. Mammoto, M. Kanapathipillai, and D. E. Ingber, Lab Chip **12**, 2175–2181 (2012).
[28]T. Zhu, F. Marrero, and L. Mao, Microfluid. Nanofluid. **9**, 1003–1009 (2010).
[29]M. Vojtisek, M. D. Tarn, N. Hirota, and N. Pamme, Microfluid. Nanofluid. **13**, 625–635 (2012).
[30]L. Liang and X. Xuan, Biomicrofluidics **6**, 044106 (2012).

[31]T. Zhu, R. Cheng, S. A. Lee, E. Rajaraman, M. A. Eiteman, T. D. Querec, E. R. Unger, and L. Mao, Microfluid. Nanofluid. **13**, 645–654 (2012).
[32]L. Liang, C. Zhang, and X. Xuan, Appl. Phys. Lett. **102**, 234101 (2013).
[33]J. Zeng, Y. Deng, P. Vedantam, T. R. Tzeng, and X. Xuan, J. Magn. Magn. Mater. **346**, 118–123 (2013).
[34]T. Zhu, R. Cheng, Y. Liu, J. He, and L. Mao, Microfluid. Nanofluid. **17**, 973–982 (2014).
[35]Y. Zhou, L. Song, L. Yu, and X. Xuan, J. Magn. Magn. Mater. **412**, 114–122 (2016).
[36]R. Zhou and C. Wang, Biomicrofluidics **10**, 034101 (2016).
[37]W. Zhao, T. Zhu, R. Cheng, Y. Liu, J. He, H. Qiu, L. Wang, T. Nagy, T. D. Querec, E. R. Unger, and L. Mao, Adv. Funct. Mater. **26**, 3990–3998 (2016).
[38]M. Hejazian and N. T. Nguyen, Biomicrofluidics **10**, 044103 (2016).
[39]S. Mitragotri and J. Lahann, Nat. Mater. **8**, 15 (2009).
[40]S. Martin, Cell Cycle **8**, 3643–3647 (2009).
[41]A. Valero, T. Braschler, A. Rauch, N. Demierre, Y. Barral, and P. Renaud, Lab Chip **11**, 1754–1760 (2011).
[42]N. M. Anstey, B. Russell, T. W. Yeo, and R. N. Price, Trends Parasitol. **25**, 220–227 (2009).
[43]M. Yamada and M. Seki, Anal. Chem. **78**, 1357–1362 (2006).
[44]S. Sugaya, M. Yamada, and M. Seki, Biomicrofluidics **5**, 24103 (2011).
[45]J. P. Beech, S. H. Holm, K. Adolfsson, and J. O. Tegenfeldt, Lab Chip **12**, 1048–1051 (2012).
[46]K. K. Zeming, S. Ranjan, and Y. Zhang, Nat. Commun. **4**, 1625 (2013).
[47]J. DuBose, X. Lu, S. Patel, S. Qian, S. W. Joo, and X. Xuan, Biomicrofluidics **8**, 014101 (2014).
[48]M. Masaeli, E. Sollier, H. Amini, W. Mao, K. Camacho, N. Doshi, S. Mitragotri, A. Alexeev, and D. Di Carlo, Phys. Rev. X **2**, 031017 (2012).
[49]X. Lu and X. Xuan, Anal. Chem. **87**, 11523–11530 (2015).
[50]X. Lu, L. Zhu, R. Hua, and X. Xuan, Appl. Phys. Lett. **107**, 264102 (2015).
[51]A. R. Kose, B. Fischer, L. Mao, and H. Koser, Proc. Natl. Acad. Sci. U.S.A. **106**, 21478–21483 (2009).
[52]Y. Zhou, D. T. Kumar, X. Lu, A. Kale, J. DuBose, Y. Song, J. Wang, D. Li, and X. Xuan, Biomicrofluidics **9**, 044102 (2015).
[53]R. E. Rosensweig, Annu. Rev. Fluid Mech. **19**, 437–461 (1987).
[54]Y. Gao, Y. C. Jian, L. F. Zhang, and J. P. Huang, J. Phys. Chem. C **111**, 10785–10791 (2007).
[55]T. B. Jones, *Electromechanics of Particles* (Cambridge University Press, London, United Kingdom, 1995).
[56]M. D. Tarn, N. Hirota, A. Iles, and N. Pamme, Sci. Technol. Adv. Mater. **10**, 014611 (2009).
[57]F. Shen, H. Hwang, Y. K. Hahn, and J. K. Park, Anal. Chem. **84**, 3075 (2012).
[58]J. Zhu, L. Liang, and X. Xuan, Microfluid. Nanofluid. **12**, 65 (2012).
[59]See https://ferrofluid.ferrotec.com/products/ferrofluid-emg/water/EMG-408/ for FerroTec Corp.
[60]J. Happel and H. Brenner, *Low Reynolds Number Hydrodynamics* (Springer Press, 1973).
[61]B. Kirby, *Micro- and Nanoscale Fluid Mechanics: Transport in Microfluidic Devices* (Cambridge University Press, 2010).
[62]T. Zhu, D. J. Lichlyter, M. A. Haidekker, and L. Mao, Microfluid. Nanofluid. **10**, 1233–1245 (2011).
[63]E. P. Furlani, *Permanent Magnet and Electromechanical Devices: Materials, Analysis, and Applications* (Academic Press, 2001).
[64]J. Zhang, S. Yan, D. Yuan, G. Alici, N. T. Nguyen, M. E. Warkiani, and W. Li, Lab Chip **16**, 10–34 (2016).
[65]C. Liu, G. Hu, X. Jiang, and J. Sun, Lab Chip **15**, 1168–1177 (2015).
[66]X. Lu and X. Xuan, Anal. Chem. **87**, 4560–4565 (2015).